University of Nebraska - Lincoln

DigitalCommons@University of Nebraska - Lincoln

Faculty Publications from the Department of Engineering Mechanics

Mechanical & Materials Engineering, Department of

2006

E(FG)²: A NEW FIXED-GRID SHAPE OPTIMIZATION METHOD

Florin Bobaru Ph.D.
University of Nebraska at Lincoln, fbobaru2@unl.edu

Srinivas Rachakonda
University of Nebraska - Lincoln

E(FG)²: A new fixed-grid shape optimization method based on the element-free Galerkin mesh-free analysis:

Taking large steps in shape optimization

Florin Bobaru and Srinivas Rachakonda

Department of Engineering Mechanics, University of Nebraska–Lincoln, Lincoln, NE 68516-0526, USA
Tel 402 472-8348, fax 402 472-8292, email fbobaru2@unl.edu

Present Address for S. Rachakonda — Olin Neuropsychiatry Research Center, Hartford, CT 06106, USA

Abstract
We propose a shape optimization method over a fixed grid. Nodes at the intersection with the fixed grid lines track the domain's boundary. These "floating" boundary nodes are the only ones that can move/appear/disappear in the optimization process. The element-free Galerkin (EFG) method, used for the analysis problem, provides a simple way to create these nodes. The fixed grid (FG) defines integration cells for EFG method. We project the physical domain onto the FG and numerical integration is performed over partially cut cells. The integration procedure converges quadratically. The performance of the method is shown with examples from shape optimization of thermal systems involving large shape changes between iterations. The method is applicable, without change, to shape optimization problems in elasticity, etc. and appears to eliminate non-differentiability of the objective noticed in finite element method (FEM)-based fictitious domain shape optimization methods. We give arguments to support this statement. A mathematical proof is needed.

Keywords: fictitious domain, element-free Galerkin, mesh-free methods, shape optimization, thermal fins, fixed grid

1 Introduction

Solving shape-optimization problems with the classical boundary variation technique requires the change of position for the discretization nodes. If the finite element method (FEM) is used in this context, the need of remeshing after *large* shape-changes that lead to mesh distortion increases the computational cost, and data transfer from the old to the new mesh introduces errors. Excessive distortion of the finite element mesh introduces numerical errors that rend the optimization iterations unreliable. Mesh-free methods have been applied to shape optimization problems to eliminate the need for remeshing (e.g., Grindeanu et al. 1999; Bobaru 2001; Bobaru and Mukherjee 2002; Kim et al. 2002; Bobaru and Rachakonda 2004a). In Bobaru

and Rachakonda (2004a), some limitations still exist for very large shape changes: nodes have to be arranged in columns for vertical shape changes to avoid the material overlap, and when the shape changes are too large, regions of very low node density may appear. In this situation, repositioning and insertion of new nodes is needed.

Fictitious domain methods also avoid remeshing. Some recent results on the application of fictitious domain methods to shape optimization problems are published in Haslinger and Mäkinen (2003), Haslinger et al. (2001a), Haslinger et al. (2001b). In these works, the FEM is used and one major problem is that the objective function can loose differentiability, as noted in Haslinger and Mäkinen (2003) pp. 187–189. In this case, special optimization algorithms for non-smooth optimization have to be used, resulting in a computational cost penalty. A combination of the fictitious domain method and moving mesh method in the FEM context is reported in Mäkinen et al. (2000), and the non-smooth objective function and locking effects observed in fixed mesh methods are apparently eliminated. Some of the advantages of the fictitious domain method, however, are lost as remeshing at the boundary becomes complex, and the discrete state equations must be formed in each iteration. Another approach to eliminating the non-smoothness of the objective function in the fictitious domain methods has been recently proposed as a geometry projection method on a regular finite element grid in Norato et al. (2004). The non-smoothness of the objective function is avoided using a problem-dependent mollification method.

In the fictitious domain method for shape optimization, computations are carried out in a fixed, auxiliary domain, Ω, of a simple shape that embeds the physical domain, ω, of the structure under analysis (see e.g., chapter 6 in Haslinger and Mäkinen 2003). Material projection methods (e.g., Garcia-Ruiz and Steven 1999; Norato et al. 2004) are special versions of the fictitious domain method in which

a material measure specifies the distribution of solid and void subregions in Ω.

The method we propose here originated in the master's thesis of Rachakonda (2003) and can be thought of as a material projection method as the physical domain, ω, is projected over a fictitious domain, Ω, and shape changes take place over a fixed-grid covering the fictitious domain (see Figure 1.) The boundary of ω is moving over the fixed grid. Discretization nodes on the moving boundary are the only nodes that "float" during the shape optimization process. With the EFG, these floating nodes can be inserted, eliminated, or simply change position with ease. The floating nodes do not require any change in the integration of the weak forms as the EFG background integration cells are not changed and are defined by the fixed grid. This process is *completely different* from remeshing used in the FEM, as in the FEM, one has to introduce new elements, and therefore, new integration points near the domain's boundary, and no simple algorithms for this local remeshing are available. Therefore, the critical feature of the proposed method is the use of a mesh-free algorithm as the solver for the analysis problem, as the EFG method allows for easy insertion/ deletion/change in position of nodes on the boundary. In this fixed-grid EFG or E(FG)^2 method for shape optimization, no special algorithm is required for adding the floating boundary nodes to the fixed grid nodes in the solution of the analysis problem. Recall that in a mesh-free solution, the integration cells are used for the purpose of integration only; they do not participate in the construction of the shape functions which are built in terms of the nodes (e.g., Belytschko et al. 1996). The integration cells that fall outside the physical domain, ω, are simply discarded from the integration of the weak form. Some cells are partially cut by the domain's boundary, and for these cells, we only use the Gauss integration points that fall inside ω. We conduct a convergence study of this procedure, and observe numerically, quadratic convergence in terms of spacing between the grid nodes. By adding the floating boundary nodes to the fixed grid nodes inside the domain, ω, when building the approximation, we insure a smooth representation of the geometry and the tools for "mesh fitting" used in Mäkinen et al. (2000) with the FEM are not necessary. The E(FG)^2 method we propose here also appears to eliminate the problem of the objective function non-differentiability shown to exist in finite element solutions of shape
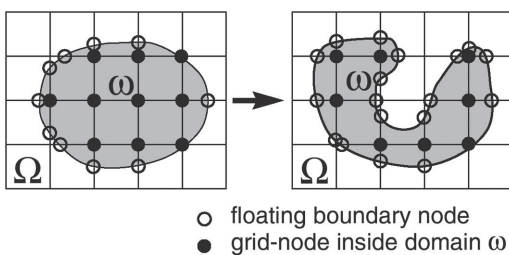

○ floating boundary node
● grid-node inside domain ω

Figure 1. A schematic representation for shape changes in the fixed-grid EFG method for shape optimization. In real situations, the grid is much finer and the number of floating boundary nodes is just a fraction from the total number of discretization nodes.

optimization problems solved by the fictitious domain method (e.g., pp. 187–189 in Haslinger and Mäkinen 2003). We claim that the reasons for this important property, for which a mathematical proof is still needed, are two:

1. The use of the floating points in the mesh-free approximation over the fixed grid and the integration scheme over the fixed cells;
2. The mesh-free shape functions create a "diffuse" (smooth) approximation which is not linked to integration cells or elements.

Recall that the precursor to the EFG method was named the "diffuse-element method" by Nayroles et al. (1992). Also, in the E(FG)^2 shape optimization method we introduce here, the need for a mollification procedure, as used in Norato et al. (2004), at the boundary of the physical domain is not needed.

Various ways of parameterizing the boundary of the domain ω can be selected with the E(FG)^2, including implicit representations (e.g., Turk and O'Brien 2002) for a general shape optimization problem. In this study, however, we test the new method on examples in which the designable boundary is described by a set of control points (design variables) which are interpolated with a shape-preserving Akima spline function. Intersections of this spline function with the fixed grid create the boundary floating nodes used in the solution. The shape optimization problems we can treat with the E(FG)^2 can have any type of boundary conditions imposed on the designable boundary. We also note that as fixed nodes and Gauss integration points falling outside ω are left out from the computation, when the shape changes result in a reduction of area (volume) of ω, important computational savings are made.

The examples we treat in detail concern the optimal shape design of thermal fins as this is a perfect benchmark for testing the ability of an optimal shape design algorithm to dealing with large shape changes (e.g. Bobaru and Rachakonda 2004a,b). The shape-optimization algorithms developed here are by no means restricted to heat-transfer problems, as they can be applied without change to examples in elasticity, etc.

There are several aspects in which the present method shows advantages compared to previous results:

– Due to the "diffuse" mesh-free approximation and to the flexibility (in inserting/eliminating nodes on the boundary of the domain) offered by the EFG mesh-free method, the non-differentiability of the objective function noticed in fictitious domain FEM-based solutions (see page 188 in Haslinger and Mäkinen 2003) appears to be eliminated. A mathematical proof of this conjecture is still needed.
– Complex schemes for local remeshing next to the boundary used in some FEM treatments of fictitious-domain shape optimization are no longer needed.
– The computation time is reduced when compared to a moving grid method as fewer nodes participate in the computation if the required shape changes shrink the domain.

– We can now relax bounds on the design variables, which needed to be imposed, to prevent extreme changes in node density developed during shape changes in the moving grid approach.
– Randomly placed nodes can now be used, as the fixed grid, with the mesh-free solution. In the moving grid mesh-free shape optimization (Bobaru and Rachakonda 2004a,b), nodes had to be organized in columns for vertical shape changes.

2 E(FG)^2: the EFG-fixed-grid shape optimization method

In this section, we describe the essence of the proposed method. At every step of the iterative, gradient-based, shape optimization process, we determine new values for the design variables that define the new position of the boundary, and we perform a geometry projection to determine the discretization nodes and the Gauss integration points that fall inside the current physical domain. The mesh-free solution is built using the fixed nodes inside the domain and the "floating" nodes on the moving boundary. Any method for computing shape sensitivities (direct differentiation, adjoint system, finite differences) can be associated with this method.

2.1 Boundary motion and new-node introduction

The idea for the fixed-grid shape optimization with the EFG method is described in Figure 1. A fixed grid of nodes and integration cells occupy a regular domain, Ω. The physical domain, ω, is projected onto Ω, and the grid nodes and Gauss points that fall inside ω participate in the computations. In addition to the grid nodes inside the domain, *floating nodes* are defined on the boundary of the domain ω, for example, at the intersection with the grid lines. The mesh-free solution procedure allows using these floating points together with the grid nodes without any special treatment. When a shape change is generated by a modification of shape design variable values, a new location of the boundary is determined, and a new set of floating nodes is formed. This set is added to the set of fixed grid nodes that fall inside the domain, ω, to participate in the discretization of the analysis problem. We note that the process described above is different from fitting the mesh to the boundary, via a remeshing procedure used in Mäkinen et al. (2000). In our method, no new "elements" or integration cells are created. We do not have to create new Gauss integration points because, in the mesh-free EFG method, the nodes are not connected to the integration cells: the approximation is separated from the integration, unlike the case of finite elements. We perform Gaussian integration of the weak form of the analysis problem using the cells defined by the fixed grid. For partially cut cells, we only use the Gauss points that fall inside the domain, as explained in Section 2.3 below.

2.2 EFG approximation for the heat transfer equations

The element-free Galerkin (EFG) (Belytschko et al. 1994) method is an improved version of the diffuse element method (DEM) (Nayroles et al. 1992). The EFG solution is built using shape functions generated with the moving least squares (MLS) approximation scheme. For details on the MLS approximation and EFG, see for example, Bobaru and Mukherjee (2001).

To be concrete, we present below the EFG approximation for the heat transfer equations. The EFG approximations for elasticity and thermo-elasticity can be seen in, for example, Bobaru and Mukherjee (2001) and (2002), respectively. The only reason we focus on the heat transfer problem is because we will test the proposed method on a challenging problem in optimal shape design of a thermal system in which very large shape changes have to be dealt with. The shape optimization method described here is applicable without any changes to problems in elasticity, etc.

The general heat-transfer problem with Dirichlet, Neumann, and Robin boundary conditions for a two-dimensional domain takes on the following form:

$$\begin{cases} \nabla \cdot (\kappa \nabla \theta) + Q = 0 & \text{in } \omega \\ \theta = \theta_0 & \text{on } \Gamma_\theta^0 \\ \kappa \nabla \theta \cdot n = \hat{q} & \text{on } \Gamma_\theta^1 \\ \kappa \nabla \theta \cdot n + h(\theta - \theta_\infty) = 0 & \text{on } \Gamma_\theta^2 \end{cases} \quad (1)$$

where κ is the thermal conductivity of the body; Q, the internal heat source; θ, the temperature; θ_0, the prescribed temperature on the Dirichlet boundary, Γ_θ^0; n, the outward normal to a boundary; $\hat{q}$, the heat flux prescribed over the Neumann boundary, Γ_θ^1; and h, the convective heat transfer coefficient over the convective boundary, Γ_θ^2. When h depends on temperature (as we will consider in our calculations), the problem becomes weakly nonlinear. A fixed-point iteration solution method can be efficiently used to linearize the problem in this case. The details of the EFG solution to the non-linear heat-transfer problem are given in Bobaru and Rachakonda (2004b), and the same scheme is used in the computations below. θ_∞ is the given ambient temperature. The dot, $(\cdot)$, in the above equations denotes the scalar (or dot-) product between tensors of rank one.

The problem in the weak form is stated as follows: *Find $\theta \in V = \{\theta \in H^1(\omega), \theta = \theta_0 \text{ on } \Gamma_\theta^0\}$ such that for every test function $\eta \in V_0 = \{\eta (H^1(\omega), \eta = 0 \text{ on } \Gamma_\theta^0\}$, we have:*

$$\int_\omega \kappa \nabla \theta \cdot \nabla \eta \, d\omega - \int_\omega Q\eta \, d\Omega - \int_{\Gamma_\theta^1} \hat{q}\eta \, d\Gamma +$$

$$\int_{\Gamma_\theta^2} h\theta\eta \, d\Gamma - \int_{\Gamma_\theta^2} h\theta_\infty\eta \, d\Gamma = 0 \text{ for any } \eta \in V. \quad (2)$$

The equalities in the definitions of the spaces V and V_0 are to be considered in the sense of trace.

The mesh-free discretization of the trial and test functions in terms of the MLS approximants are:

$$\theta(\mathbf{x}) = \sum_{I \in C} \Phi_I(\mathbf{x})\, \theta_I$$

$$\eta(\mathbf{x}) = \sum_{J \in C} \Phi_J(\mathbf{x})\, \eta_J \tag{3}$$

where C is the set of nodes that cover, with their corresponding approximation function supports, the point x, θ_I is the approximations to the nodal temperatures, and the MLS shape functions are evaluated by

$$\Phi_I(\mathbf{x}) = \mathbf{P}(\mathbf{x})^T \mathbf{A}^{-1}(\mathbf{x}) \mathbf{b}_I(\mathbf{x}). \tag{4}$$

Here, we use a linear basis in 2D, given by

$$\mathbf{P}(\mathbf{x}) = [P_1(\mathbf{x}), P_2(\mathbf{x}), P_3(\mathbf{x})]^T = [1, x, y]^T. \tag{5}$$

In Equation (4), the matrix $\mathbf{A}$ and the vector $\mathbf{b}_I$ are given by:

$$\mathbf{A}(\mathbf{x}) = \mathbf{P}^{-1}\mathbf{W}(\mathbf{x})\mathbf{P}$$

$$\mathbf{B}_I(\mathbf{x}) = [P_1(\mathbf{x}_I)\, w\,(\mathbf{x} - \mathbf{x}_I), P_2(\mathbf{x}_I)\, w\,(\mathbf{x} - \mathbf{x}_I),$$
$$P_3(\mathbf{x}_I)\, w\,(\mathbf{x} - \mathbf{x}_I)]^T$$

with w being a weighting function with compact support, and the matrices $\mathbf{P}$ and $\mathbf{W}$ having the form:

$$\mathbf{P} = \begin{bmatrix} P_1(\mathbf{x}_{c1}) & P_2(\mathbf{x}_{c1}) & P_3(\mathbf{x}_{c1}) \\ P_1(\mathbf{x}_{c2}) & P_2(\mathbf{x}_{c2}) & P_3(\mathbf{x}_{c2}) \\ \cdot & \cdot & \cdot \\ \cdot & \cdot & \cdot \\ \cdot & \cdot & \cdot \\ P_1(\mathbf{x}_{c_m}) & P_2(\mathbf{x}_{c_m}) & P_3(\mathbf{x}_{c_m}) \end{bmatrix}$$

$$\mathbf{W}(\mathbf{x}) = \begin{bmatrix} w_{c1}\,(\mathbf{x} - \mathbf{x}_{c1}) & \ldots & 0 \\ 0 & \ldots & 0 \\ \cdot & \cdot & \cdot \\ \cdot & \cdot & \cdot \\ \cdot & \cdot & \cdot \\ 0 & \ldots & w_{c_m}\,(\mathbf{x} - \mathbf{x}_{c_m}) \end{bmatrix}$$

The indexes, $\{c_1, \ldots, c_m\}$, correspond to the indexes of nodes in set C, which cover with their supports the evaluation point, $\mathbf{x}$.

A quartic spline with radial support is used in our computations as weighting function for the MLS approximants (e.g., Bobaru and Mukherjee 2002). We impose the Dirichlet boundary conditions using the transformation method from Chen and Wang (2000) and implemented in the case of heat transfer equations in Bobaru and Rachakonda (2004a).

One important property of the MLS approximation with great impact in our fixed grid shape optimization scheme is that the approximation in (3) is in $\mathcal{C}^{min(p,q)}(\omega)$, where p and q are the degrees of smoothness for the basis functions in (5), and the weighting function, respectively. In our case, as the quartic spline is $\mathcal{C}^2(\omega)$, the MLS approximation will have the same smoothness. As the shape func-

tions in (4) are nodal-based and not element-dependent, the approximation is "diffuse." In other words, the EFG shape functions or their derivatives do not have discontinuities at the integration cell boundaries, as it is the case in finite elements. Our conjecture is that this "diffuse" mesh-free approximation together with the high smoothness of the approximants, effectively eliminates the problem of non-differentiable objective function observed in finite element fictitious domain methods (Haslinger and Mäkinen 2003) for shape optimization. While a mathematical proof of this assertion is still needed, we note that as shown in Haslinger and Mäkinen (2003) pp. 187–189, the source of non-differentiability of the objective in terms of the shape design variables in fixed-grid methods with non-fitted FEM meshes is the jumps in the FEM derivatives of the shape functions at the element boundaries.

A quadratic basis can be used instead of (5) to improve convergence, but this would penalize efficiency and the gains in convergence rate do not justify it. Several studies show that using a linear basis is effective (e.g. Belytschko et al. 1996; Rabczuk and Belytschko 2005), and this basis will be used in all our numerical examples.

Normally, the integrals over ω are computed using Gaussian integration over a set of *background cells that overlap the domain exactly*. Here, we use a different approach for integration and this is explained in the next section.

2.3 Geometry projection for integrating the EFG weak form

The discussion below is limited to the two-dimensional case in which the designable boundary curve is given by a function of one variable (the *x*-coordinate in Figure 2). The method is easily extended to the case in which the designable boundary is a general curve in 2D or a surface in 3D.

The domain occupied by the physical body is bounded by its boundary curve (or surface in 3D). The domain is overlapping a fixed grid, as depicted in Figure 2 for the case of a quarter of a disk for which the designable boundary curve is defined by the function, $f(x) = (1 - x^2)^{1/2}$. We take the fixed grid cells over Ω to play the role of the background integration cells used for integrating the weak form over ω. The EFG discretization nodes are the grid nodes. While the choice above is convenient and simplifies the data structures, other choices for the nodes and the background integration cells are possible.

New "floating" nodes are defined at the points where the design boundary curve intercepts the integration grid lines. The coordinates of these points are easily determined in the examples we consider in Sections 3 and 4, as we employ the Akima interpolating spline through the design variables. The *y*-coordinates of the points that control the shape of the Akima spline are the design variables in the shape optimization algorithm. The design points are completely independent from the grid nodes. In the current implementation, we find the "floating" boundary nodes at the intersections between the vertical grid lines and the boundary spline curve. As the boundary is given by a one-dimensional function, the intersection between a vertical grid line and the boundary *is unique*.
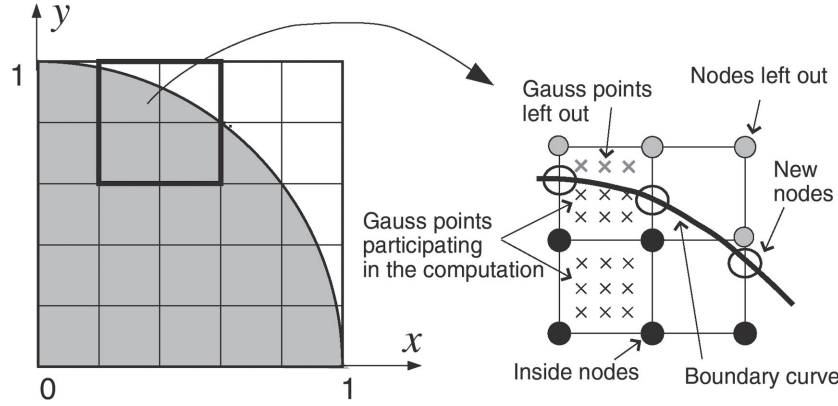
Figure 2. The geometry projection scheme. "Floating" nodes are placed at the intercepts between the boundary curve and the vertical grid lines. The mesh-free approach allows for easy introduction of these new nodes. Note that a similar FEM solution would have to deal with complex algorithms for creating new elements at the boundary. In our case, no new cells and integration points need to be created; nodes and Gauss points outside the physical domain are left out from the computation. The geometry projection scheme proposed shows quadratic convergence in terms of the grid spacing when evaluating domain integrals [see (8)]. In the computations we use 5 × 5 integration in each cell.

With the boundary nodes assigned, we determine if a Gauss point is to be used in the integration of the weak form by finding whether the Gauss point is inside or outside the domain. This can be done, for example, by comparing the y-coordinate of the current Gauss point (x_G, y_G) with the value of a spline function, s, interpolating the boundary nodes, evaluated at x_G:

if $y_G - s(x_G) < 0$ then use this Gauss point   (6)

The numerical integration of domain integrals in the weak form in (2) is performed using the fixed grid integration cells following the algorithm below:

Algorithm 1 Geometry projection in E(FG)²: computing a domain integral such as those in (2)

1: determine location of boundary nodes
2: find the set S of nodes inside domain ω and on the boundary
3: **for all** integration cells with at least one node inside domain ω **do**
4:     **for all** Gauss points (xG, yG) inside integration cell **do**
5:         **if** $yG - s(xG) < 0$ **then**
6:             search neighboring nodes in S that cover this Gauss point (form set C of covering nodes)
7:             **for all** nodes in C **do**
8:                 compute shape function and derivatives at Gauss point
9:                 assemble contributions to global matrix
10:             **end for** nodes in C
11:         **end if**
12:     **end for** Gauss points
13: **end for** integration cells

One important advantage of the fixed-grid algorithm for shape optimization is that the smaller the domain, ω, is, the faster the computation becomes. Cells that have no node inside the boundary are skipped from the computations altogether. The scheme described above is schematically represented in Figure 2. When the body becomes non-convex, a neighboring search algorithm like the one proposed by Duarte (1996) has to be used to find the set of nodes that cover with their supports a certain Gauss point.

2.4 Convergence results for the geometry projection method

We test the convergence properties of the procedure described above by evaluating a domain integral. Ω, is the unit square in Figure 2, while the physical domain, ω, which is to be integrated over, is the quarter disk. The exact value of the domain integral over ω is:

$$\frac{\pi}{4} = \int_0^1 \sqrt{1 - x^2}\, dx = \int_\omega dx\,dy \qquad (7)$$

The approximation based on the Algorithm 1 described in section 2.3 is computed as:

$$\int_\omega dx\,dy \approx \sum_{\text{cells} \in \mathcal{C}} \int_{-1}^1 \int_{-1}^1 J(\xi, \zeta)\, d\xi\, d\zeta =$$
$$\sum_{\text{cells} \in \mathcal{C}} \left(\sum_{j \in \mathcal{G}} \sum_{k \in \mathcal{G}} w_j\, w_k\, J(\xi_j, \zeta_k) \right) \qquad (8)$$

where $\mathcal{C}$ is the set of cells that have at least one node inside the domain, ω, and the set, $\mathcal{G}$, is the set of Gauss points that fall inside ω. The parameters, w_j, w_k, ξ_j, and ζ_k are the usual Gaussian integration weights and Gauss nodes in the parent domain, and J is the Jacobian transformation.

We introduce the approximation error by cutting the integration cells and using only those Gauss points that fall inside the domain. As we see next, the *numerical* order of approximation with this procedure is quadratic in the limit of vanishing grid spacing.

In the numerical convergence tests of the geometry projection discussed above, we compute the relative error as

$$e = \frac{|A_{\text{approx}} - A_{\text{exact}}|}{A_{\text{exact}}} \qquad (9)$$

where A_{exact} is the exact value of the integral in (7) and A_{approx} is the value computed with the geometry projection EFG method as an area integral over the quarter disk
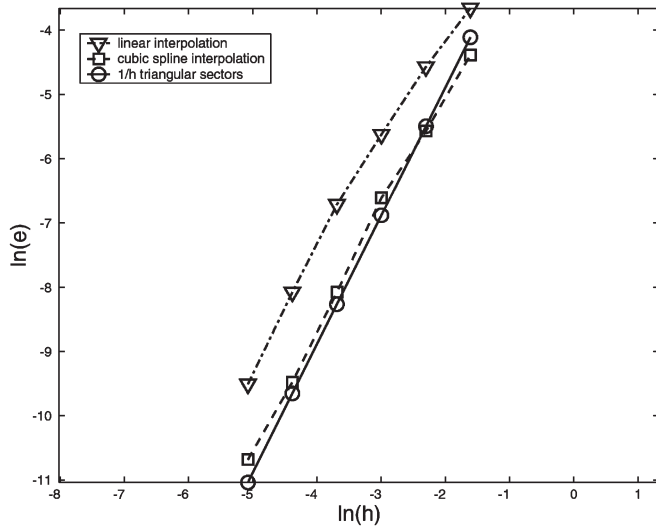
Figure 3. The relative error computed as in (9) vs. the grid spacing. Superlinear to quadratic convergence is achieved in numerically integrating the domain using the cutting strategy described in Figure 2.

in Figure 2. We use grid spacings h equal to 1/5, 1/10, 1/20, 1/40, 1/80, and 1/160, respectively. The variation of the relative error, e, vs. the grid spacing is shown (in a log–log plot) in Figure 3. We use linear spline and Akima spline interpolation in (6) to determine if a Gauss point is inside or outside ω. The convergence becomes quadratic for the denser grids. Notice that the quadratic convergence is the *analytical rate* for approximating the disk area with triangular sectors spanning equal angles. The number of sectors used for the plot in Figure 3 is $1/h$, that is, 5, 10, 20, 40, 80, 160, respectively. In the computations that follow, the Akima spline interpolation will be used in (6) for computing integrals over the domain.

2.5 Fixed-grid shape optimization with EFG

With this simple geometry projection for computing the solution over the physical domain, ω, the algorithm for EFG fixed-grid, E(FG)^2, shape optimization is proposed:

Algorithm 2. E(FG)^2: the EFG fixed-grid shape optimization method

---

1: define initial guess for design variables (control points for the boundary spline function)
2: **while** not a local minimum **do**
3:   find objective function, constraints by solving (2) using EFG method and Algorithm 1 over ω
4:   compute sensitivities of objective function, constraints, with method of choice
5:   optimizer provides new values for design variables
6:   update control points for boundary spline
7: **end while**

The sensitivities can be computed in various manners: by direct-differentiation method, adjoint system, or by finite differences. In the example we present below, we use an sequential quadratic programming (SQP) optimizer

from the International Mathematical and Statistical Library (IMSL) that internally computes sensitivities by finite differences. This choice is made here for convenience only.

This algorithm is clearly applicable to not only shape optimization problems for thermal systems but to any shape optimization problems whose equations of state are described by PDEs, such as optimal shape design of elastic and thermoelastic bodies under stress constraints.

3 Test problem for shape optimization involving large shape changes

A challenging test in optimal shape design is the shape optimization of cooling fins. The problem is treated in, for example, Bobaru and Mukherjee (2002); Bobaru and Rachakonda (2004b). When starting from a generic regular shape of the cross-sectional area of the thermal cooling system, large shape changes between the initial and final design take place.

We analyze a section of a long fin array and use periodic boundary condition. One face of the thermal system is attached to a body at constant temperature, while the opposite face is exposed to the cooler temperature of the ambient air (Figure 4). We solve the shape optimization problem on the top cross-section of the cooling system. The boundary conditions on the cross-section of the thermal system are shown in Figure 4. The following values are used in (1) : $\theta_0 = 500K$, $\theta_\infty = 300K$, and $q = 0$ (due to periodicity conditions). Even if the shape optimization problem is set in two dimensions, the solution takes into account the third dimension via the dependence of the heat transfer coefficient on the height of the fin. We consider the heat transfer coefficient as a function of the boundary temperature:

$$h(z, \theta) = \frac{2\kappa \, \mathrm{Pr}^{1/2}}{z \, [336(\mathrm{Pr} + 5/9)]^{1/4}} \, [\mathrm{Gr}(z, \theta)]^{1/4}. \qquad (10)$$

Here, z is the coordinate along the height of the fin, Pr is Prandtl's number, and Gr is Grashof's number. The heat
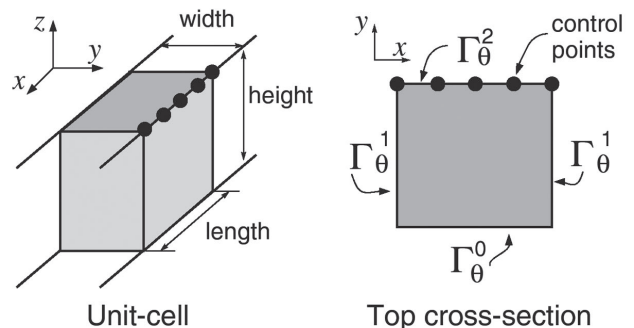

Figure 4. The imposed temperature boundary, (Γ_θ^0), zero-flux boundary, (Γ_θ^1), and the convective boundary, (Γ_θ^2). Design variables (control points) are interpolated with a shape-preserving Akima spline and are selected on Γ_θ^2 only (including its ends); as a result, the zero-flux, Γ_θ^1, boundaries can change their length but not shape. Symmetry is imposed about the middle vertical axis.

transfer coefficient depends on Grashof's number which implies a dependence on the fin's temperature on Γ_θ^2, as

$$\mathrm{Gr}\,(z, \theta) \;=\; \frac{g\beta(\theta - \theta_\infty)z^3}{\nu^2} \tag{11}$$

The dependency of h on $\theta_{|\Gamma_\theta^2}$ is more complicated than the root-four behavior apparent from (10) and (11). That is because the Prandtl number and the convective factor, $g\beta/\nu^2$, in Grashof's number also vary with the temperature θ on Γ_θ^2 (see Table 1 in Bobaru and Rachakonda 2004a). The values we use for the ambient are those of air at one atmosphere and for the range of temperatures and conditions specified above. The ambient fluid properties are captured by the "convective term," $g\beta/\nu^2$. These properties are normally evaluated at the film "average" temperature $\theta f = (\theta_w + \theta_\infty)$ as described in White (1988), page 298, where θ_w is the "wall" temperature, i.e., the temperature of the fin's convective boundary.

The mathematical form of the optimization problem is to find the shape of the fin cross-section that solves:

$$\min F(\mathbf{y}) = -\kappa\,\frac{\int_{\Gamma_\theta} q\,d\Gamma}{L_{\mathrm{fin}}}\;,\; \mathbf{y} \in \omega \tag{12}$$

subject to

$$H_1(\mathbf{y}) = 1 - \frac{\int_\omega d\omega}{A_{\max}} \geq 0 \tag{13}$$

$$H_2(\mathbf{y}) = 1 - \frac{\mathrm{BLO}}{\mathrm{BLO}_{\max}} \geq 0 \tag{14}$$

where q is the heat flux from the base, L_{fin} is the length of the base of the fin, $\mathbf{y} = [y_1, \ldots, y_p]$ is the design vector representing the y-coordinates of the control points on the spline boundary. The domain, ω, is defined by $\{\mathbf{y} \in \mathbb{R}^p : 0.005 \leq y_i \leq 0.05, \forall i = 1, \ldots, p\}$. The upper bound is chosen arbitrarily. Notice that in the moving grid approach used in Bobaru and Rachakonda (2004a,b) we were forced to use a higher lower bound for the design variables due to the large difference in node density created after large shape changes. In the present fixed-grid method, the only limitation is given by the fineness of the discretization. For the discretization we use, we select the lower bound such that at least a few node layers are covered between convective boundary and the base of the fin. This insures an accurate computation of the heat- flux through the base. $A_{\max}$ is 60% of the original rectangular area. BLO is the *"boundary layer overlap"* which is the area shown in Figure 5.

Table 1 Coordinate values of the starting guess (in meters) for the design variables (d.v.'s) used to obtain the optimal shapes in Figures 10 (sharp fins) and 11 (round fins)

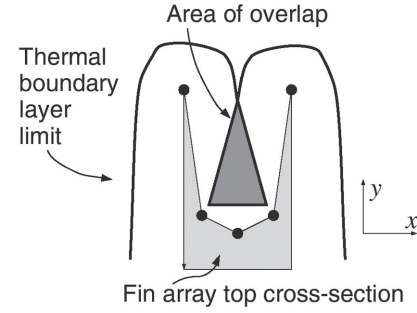| d.v.'s x-coordinates (m)	d.v.'s y-coordinates sharp fins case (m)	d.v.'s y-coordinates round fins case (m)
0.0×10^{-2}	5.0×10^{-2}	4.2×10^{-2}
1.0×10^{-2}	4.9×10^{-2}	4.5×10^{-2}
2.5×10^{-2}	5.0×10^{-2}	5.0×10^{-2}

Figure 5. Overlap area for the thermal boundary layer for two fins too close to one another. Instead of having the ambient cooling air at the limit of the boundary layer, the fins are facing each other's thermal layer of a higher temperature; thus, reducing the heat transfer.

Instead of directly evaluating this area, we compute an equivalent measure of it using a fast algorithm introduced in Bobaru and Rachakonda (2004a), based on the x-coordinates of nodes along the design boundary. A small violation is allowed in BLO$_{\max}$ with a value equal to 5% of the fin base length.

The minimization problem (12)–(13) is ill-posed in the sense that the more design variables are assigned, the more fins are created with a shape that produces a better and better objective. This aspect of the problem has been discussed in Bobaru and Rachakonda 2004a with the moving grid approach. Imposing a constraint on the length or on the curvature of the design boundary to regularize the problem would be misleading: first, the length of the boundary should be part of the solution, and second, the boundary should be allowed to have non-differentiable points. In fact, we noticed (Bobaru and Rachakonda 2004b) that the best shape for highly conductive materials is given by pointed fins.

In Section 4.1 we show that the newly introduced method is insensitive to biased grids and that we can perform large shape changes in a single iteration. The EFG fixed-grid method eliminates the need for special arrangements of nodes required in the moving grid method (Bobaru and Rachakonda 2004a,b). In section 4.2, the E(FG)² method allows us to enlarge the bounds on the design variables, and thus, uncover a new property of the optimal shapes for low and highly conductive materials; in section 4.3, we eliminate boundary overlap for low conductivity periodic fins by introducing a new zero-slope constraint. The E(FG)² helps us observe new properties for the conductivity-dependence of the optimal shape.

4 Numerical results

4.1 Area constrained optimization; biased grids

We test the new E(FG)² shape optimization method for the problem with area constraint only (12)–(13) on a part of an infinite-length thermal system by using periodic boundary conditions (no-flux though Γ_θ^1 boundaries in Figure 4).
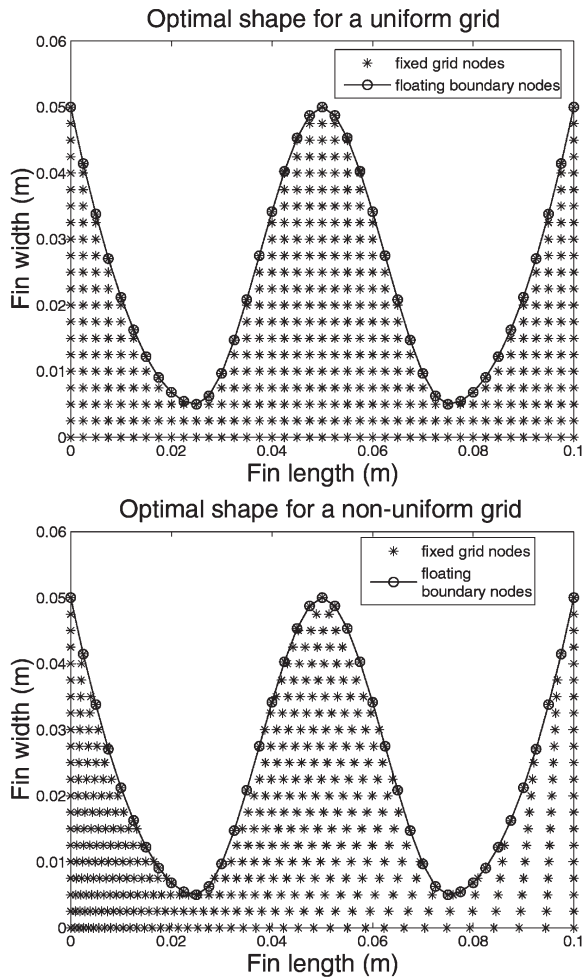
Figure 6. Insensitivity of the optimal shapes with the discretization grid: the case of a uniform grid (*top*) and a horizontally biased nonuniform grid (*bottom*). Five design variables, equally spaced in the horizontal direction, are selected on the convective boundary. Total number of nodes is the same in both cases, (21 × 41). New boundary nodes are created as in Figure 2.

Figure 7. A single optimization iteration is required from the starting guess shape (*top*) to the final finned shape (*bottom*) of the thermal system cross-section. The large shape changes involved are easily dealt with by the mesh-free fixed-grid method.

The dimensions for the cooling system are (see Figure 4): fin length is 1×10^{-1} m, fin width is 5×10^{-2} m, and the height is selected to be 4×10^{-1} m, such that it does not lead to a turbulent thermal boundary layer in natural convection conditions anywhere along the height of the system. Recall that the third dimension enters the 2D equations via the heat transfer coefficient (10).

The proposed shape optimization procedure is insensitive to biased grids. To verify this, we solve the optimization problem for the fin above with symmetry conditions on the design variables. In this test, we use a grid of 21 × 41 nodes for the fixed grid over the rectangular domain Ω of 1×10^{-1} m by 5×10^{-2} m and five design variables (control points) with their x-coordinates equally spaced along the convective boundary. The control points do not have to be grid nodes. The design variables control the profile of the convective boundary as described above. Figure 6 shows the optimal shape when no boundary layer constraint is used and when we impose a strong bias on the horizontal arrangement of the nodes. Note that as the integration
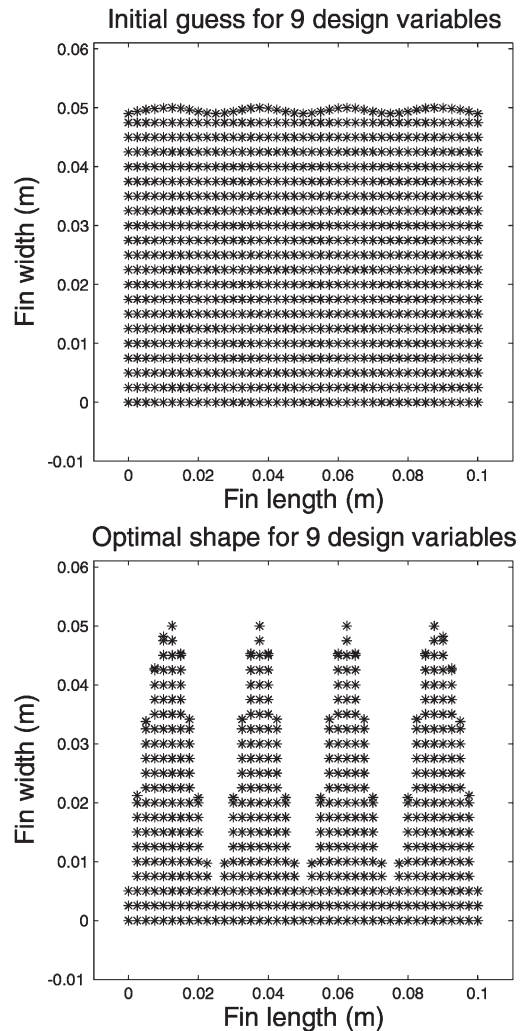
cells are fixed, we no longer have to solve the optimization problem on grids in which the nodes are arranged in "columns" as in Figure 3 in Bobaru and Rachakonda (2004a). This is an important generalization and advantage compared to the moving grid approach. Convergence to the optimal shape, which is given by a design vector with values alternating between the lower and upper bounds [0.5, 0.05, 0.5, 0.05, 0.5] × 10^{-1} m, is achieved in *a single iteration* from a slightly perturbed rectangular original shape defined by the guess design vector, [0.5, 0.49, 0.5, 0.49, 0.5] × 10^{-1} m.

When no boundary layer constraint is imposed, the ill conditioning of the problem is manifested by the increase in the number of fins, thinner and closer to one another, with the increase in the number of design variables. This has been observed before in the shape optimization with EFG based on the moving grid method in Bobaru and Rachakonda (2004a). The new fixed-grid method recovers that results, but in addition, it allows us to eliminate the requirement for a high lower bound, the moving grid method had to impose on the design variables. We can
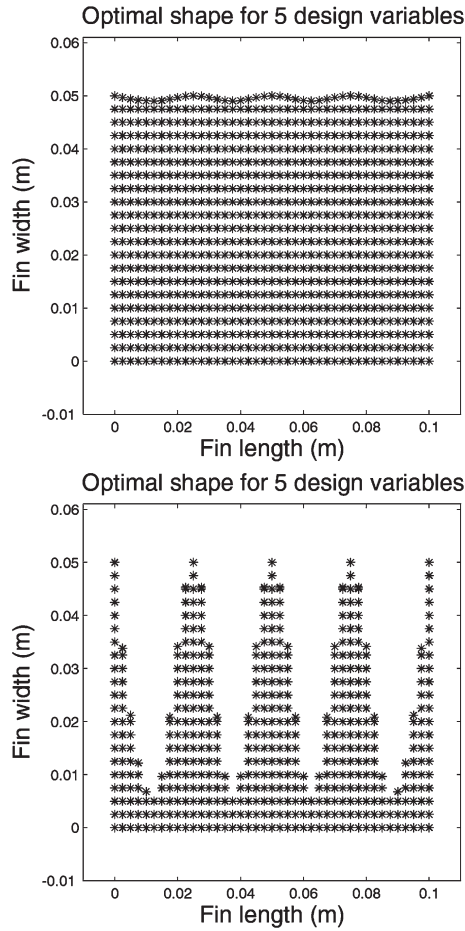
Figure 8. The first (*top*) and second and last (*bottom*) iterations for nine design variables. Notice that the formation of very thin fins at the zero- flux boundaries where colinear nodes will eventually degrade the EFG solution. In the computation of the EFG shape functions (4), each Gauss point involved in the computation needs to be covered by the supports of at least three non-colinear nodes.

Figure 9. The first (top) and second (bottom) and last iterations for 13 design variables. The number of fins increases unlimited with the increase of the number of design variables. The objective value continues to "improve" since the thermal boundary layer is not taken into account.

now handle very large shape changes between consecutive iterations. The moving grid method could deal with moderately large shape changes only.

   With nine design variables, the optimal shape shown in Figure 7 gives a better objective function value. By changing the initial perturbation from the rectangular shape so that the middle design variable is on a "hill" rather than in a "valley" as in Figure 7, we obtain the results in Figure 8. Notice that in this case, the fins at the extremities present regions of only colinear nodes. The EFG solution can break down in such cases (see, e.g., Belytschko et al. (1994)), and to avoid this, the supports for adjacent nodes have to be increased. This process degrades the accuracy of the solution as we loose the localization properties of the approximation. A denser grid is required in such situations.

   When even more control points are chosen on the convective boundary, more fins form for an even better value of the objective function. The case of 13 design variables is in Figure 9. The grid size is kept the same in all these case of 5, 9, and 13 design variables. The values of the objective function (negative heat flux) are not physical, as the model
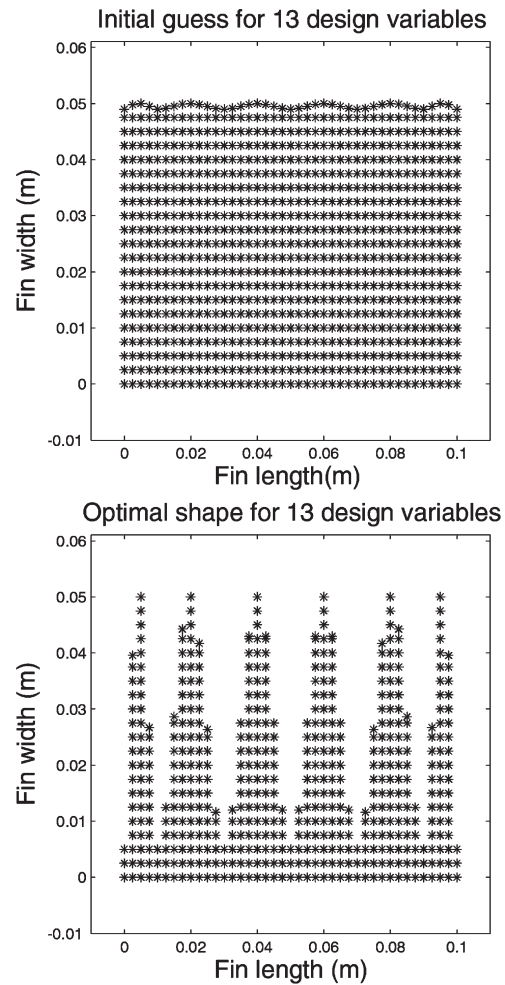
assumes that all points on the convective boundary are exposed to the ambient temperature. This, however, is not possible if the fins that are generated are too close to one another due to the presence of the thermal boundary layer that forms along the height of the fins. A constraint, such as the one in (14), has to be used for a physically correct model.

4.2 Boundary layer overlap constrained optimization

   The constrained optimization problem (12)–(14) is well-posed as fins cannot be generated *ad infinitum* due to the overlap of the thermal boundary layer. We now select a *unit cell* of length 5×10^{-2} m for reasons presented in Bobaru and Rachakonda (2004a). The third dimension, z, enters the solution in two ways: firstly, through the convective boundary condition as the heat transfer coefficient, h, depends on the height, and secondly, through the thickness of the boundary layer which is used to compute the boundary layer overlap in (14). A fixed grid with 31×31 nodes is used for the rectangular area, Ω, of 5×10^{-2} m by 5×10^{-2} m.
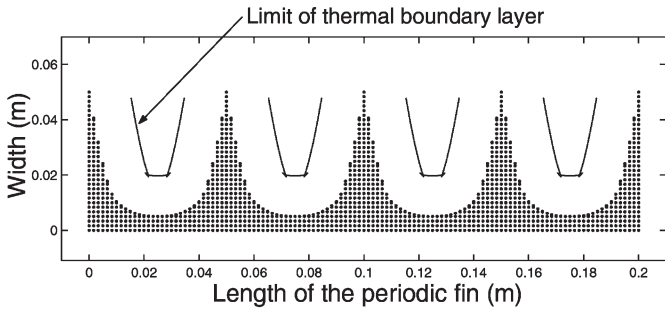
Figure 10. The optimal configuration for the periodic fin of a highly conductive material. Five design variables are selected on the unit cell. The control points oscillate between the their lower and upper bounds. The area constraint, however, is not active. As the temperature does not drop significantly while heat is transported across the fin, it is beneficial to create "infinite length bounding a finite area" shapes to maximize the heat flux through the fin.
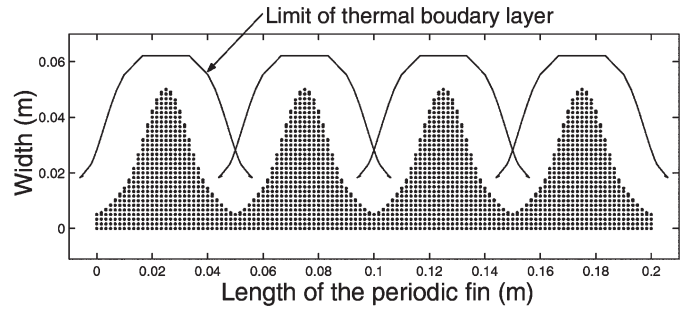
We use five design variables selected on the convective boundary. Four copies of the unit cell optimal shape are repeated to construct the periodic fin array shown in Figures 10 and 11 which are obtained with the starting guesses for the design variables as in Table 1. We give only the first three coordinates as we use symmetry of the geometry for the remaining two design variables.

For the unit-cell, the history of the objective function, area constraint, and thermal boundary layer overlap (BLO) constraint for the highly conductive material (aluminum with $\kappa = 235$ W/mK) are given in Figures 12, 13, and 14, respectively. While the boundary layer overlap is eliminated in the unit cell, the value of the objective function reached by the rounded tip fins is overstated for the periodic construct due to the overlap of the thermal boundary layer resulting when the unit cells are joined together. Notice that for the highly conductive material, the sharp fin shape uses only 48% of the maximum area allowed, while the round fin shape uses 80% of the same value. The sharp fins, there-

Figure 11. An optimal configuration for the periodic fin of a highly conductive material. Five design variables are selected on the unit cell. The area of the cross-section used is 40% larger than the sharp fin solution, while the heat flux through the base is 8% less than the sharp fins. The periodic array has some overlap of the thermal boundary layer which can be eliminated by imposing zero-slope end conditions for the interpolated design boundary.

fore, use 40% less material while providing a value of the objective function 8% higher than the round profile. The control points oscillate between their lower and upper bounds. The area constraint is not active. As the temperature does not drop significantly (less than 0.5%) while heat is transported across the fin for this highly conductive material, it is beneficial to create shapes with as much conductive boundary length as possible enclosing the finite cross-sectional area to maximize the heat flux through the fin. The only limiting factors here are the boundary layer overlap constraint and the simple bounds on the design variables themselves.

We now use a hypothetical material with a low thermal conductivity value, $\kappa = 1$ W/mK. An optimal shape for the unit cell is shown in Figure 15. The area constraint is *active*, but in contrast to the highly conductive case, the design variables stay away from their upper bounds. The optimal shape, in this case, is determined such that the top cross-section of the cooling system does not extend narrow
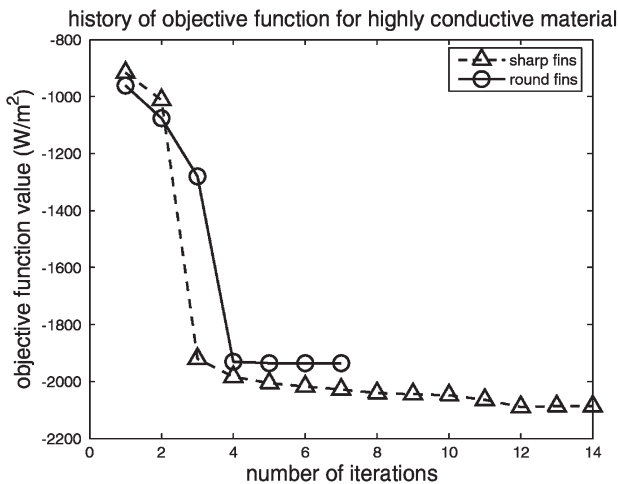

Figure 12. The objective function history for two initial configurations that lead to the optimal shapes shown in Figures 10 and 11. A lower value is better.
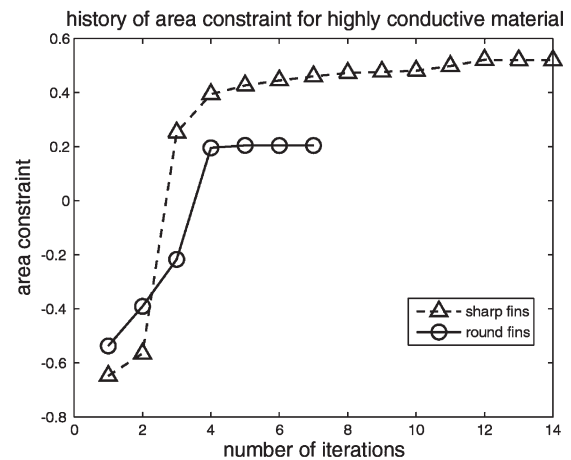

Figure 13. The history of the area constraint (13) for highly conductive material. A larger value means less area is used. A positive value means the area used is less than the maximum allowed value. The sharp fin design uses 40% less material than the rounded shape design.
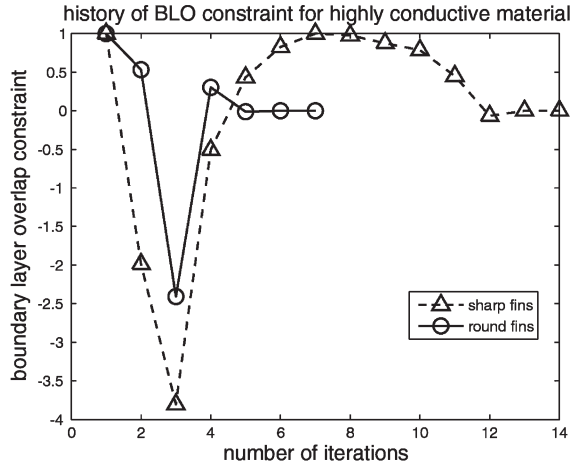
Figure 14. The history of the boundary layer overlap constraint (14) for the material with high conductivity.

Figure 15. An optimal configuration for the unit-cell fin of a low conductivity material when five design variables are used on the design boundary. The area constraint is active. As the temperature on the convective boundary drops compared to the based temperature when heat transfer to the ambient competes with the heat conduction from the base, it is not beneficial to create narrow elongated shapes that can reduce heat transfer, and thus, decrease the heat flux. In this optimal design (local), the control points stay away from their upper bounds.

fins that would cool too much and, with their reduced surface temperature, limit the effectiveness of the heat-transfer with the ambient [see (10) and (11) for the connection between $\theta_{|\Gamma_\theta^2} - \theta_\infty$ and heat-transfer coefficient].

In our previous work using a moving grid method, we were not able to use lower values for the design variables' lower bound, and the unit conductivity local optimal shape we determined did not make use of all allowable area (see Table 3 in Bobaru and Rachakonda 2004b). The boundary layer overlap constraint induces a large number of local minima in the problem. With the lowering of the lower bound permitted by the new $E(FG)^2$ method, we can attain a better objective function value than before and also observe an interesting property of low conductivity materials; the amount of material used by the optimal top cross-section is maximized to prevent drastic cooling that reduces heat transfer. In Table 2, we compare the results obtained with the moving grid in Bobaru and Rachakonda (2004b) and those with the current $E(FG)^2$ for the low conductivity material. Using the same starting guess but having different lower bounds for the design variables in the moving grid and the fixed grid, the latter improves the objective value by almost 15% with an increase in the use of area of 9%. The shape, however, that activates the area constraint (uses 100% of the allowed cross-sectional area) provides the best value of the objective function. The final shape obtained with "guess B" in Table 2 is used for the plot in Figure 15.

Notice that the fin in Figure 15 induces significant boundary layer overlap if repeated by periodicity. One solution for eliminating the overlap is to space the fins to twice the thickness of the boundary layer at the point where the adjacent layers come in contact. Another option is to use a constraint on the geometry requesting the slope of the boundary curve to be zero at the ends of the fin. The latter is analyzed next.

4.3 Smooth-shape constraints for periodic array: low conductivity materials case

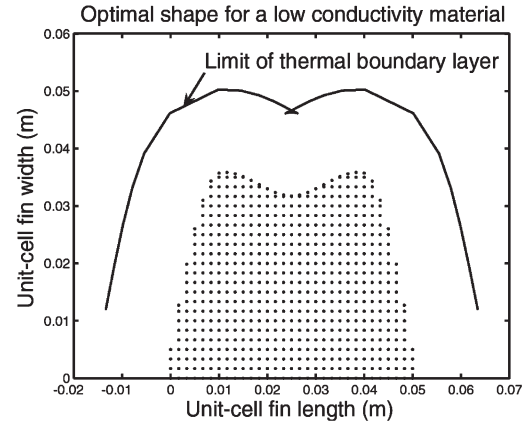For the non-sharp shapes, it seems reasonable to impose a zero-slope condition at the ends of the interpolating spline. In the moving grid solution (Bobaru and Rachakonda 2004b), the discretization nodes at the ends of the design boundary are forced to take on the same y-coordinate. In the present case, this is not possible as the nodes are fixed. Moreover, one cannot impose an end condition on shape-preserving splines. The end conditions for these splines are determined automatically to preserve the "aspect" of the interpolated points.

Here, we introduce a control point (design variable) close to the end-control point (we still use symmetry) and choose to impose a geometric constraint in addition to (13) and (14), such that the first two design variables have similar y-coordinates. When the design variables are then interpolated with the shape-preserving spline, we will approximately satisfy the zero slope at the ends of the convective boundary, which eliminates boundary layer overlap. The added constraint is:

$$H_3(\mathbf{y}) = (0.001 - |y_1 - y_2|) * s \tag{15}$$

where s is a scaling factor taken equal to 500. The constraint becomes active when the first two design variables differ from each other by more than 2% when they are close to their upper bound or 20% when they are close to their lower bound. We select two different starting guesses as detailed in Table 3:

case 1   starting values are close to their lower bounds
case 2   shift upwards the values in case 1 (by 2 cm) so that starting values are closer to their upper bounds

These two different starting guesses lead to the optimal shapes shown in Figure 16.

Observe that the shapes obtained are similar to each other, the only difference being that in case 1 (starting closer to the base of the fin), the optimal shape stays closer

Table 2. Comparison of the influence of the design variables bounds on the qualitative solution for low-conductivity materials. Results with lower bound (LB) of 0.015 m are obtained in Bobaru and Rachakonda (2004b). The values of the objective function and constraints are shown for the optimal design.

Test case d.v.'s (m)	Starting values for d.v.'s (m)	Final values for (W/m²)	Heat flux (-$F(\mathbf{y})$) final value final value	Area constraint final value	Percentage of allowed constraint area	Boundary layer overlap
Moving grid [a] (LB 0.015)	4.2×10^{-2} 4.5×10^{-2} 5.0×10^{-2}	1.5×10^{-2} 2.8×10^{-2} 4.65×10^{-2}	1253.6	1.1×10^{-1}	89%	-0.55×10^{-3}
Fixed grid guess A (LB 0.005)	4.2×10^{-2} 4.5×10^{-2} 5.0×10^{-2}	0.50×10^{-2} 3.41×10^{-2} 3.17×10^{-2}	1435.6	3.1×10^{-2}	97%	0.9
Fixed grid guess B [b] (LB 0.005)	1.0×10^{-2} 2.40×10^{-2} 4.95×10^{-2}	0.50×10^{-2} 3.57×10^{-2} 3.17×10^{-2}	1483.4	3.3×10^{-14}	100%	0.3×10^{-1}

a. Results from Table 3 in Bobaru and Rachakonda (2004b)
b. This starting guess is a perturbation of the final shape obtained with the moving grid method in Bobaru and Rachakonda (2004b)

to the base and uses less area, yet produces a similar heat transfer value as that from case 2. The more extended fins, produced using case 2, result in lower convective boundary temperatures that, in turn, reduce the heat transfer. The reason for which the objective function value is not lower in case 2 than in case 1 is that the cross-sectional area and the length of the convective boundary at the final iteration are larger in case 2 than in case 1. This can be seen from the data in Figure 17 and Table 2.

Unfinned local minimizers are also obtained for the case of low conductivity material under certain initial guesses. Such a local minimum is obtained with all design variables touching their lower bounds, closest to the heat source. The value of the objective function, however, is better for the designs shown above. There is, of course, a certain value of the material conductivity that renders the unfinned thermal system as the global minimizer.

5 Conclusions

We presented a new shape optimization method based on a mesh-free solver, the element-free Galerkin method. The new method performs shape changes over a fixed grid in which the domain of interest is imbedded (projected). A set of "floating" nodes that discretize the boundary are the only ones that move, their positions being determined by the shape design variables (control points) on the design boundary at the intersections between the boundary curve and the fixed grid. The combination of the projection onto

the fixed grid and the EFG solver led to the new E(FG)² shape optimization method in which:

1. the floating nodes are easy to deal with as they do not introduce any complexity in the solution procedure.
2. the non-smoothness of the objective function observed in FEM-based fictitious domain methods appears to be eliminated due to the "diffuse" type and higher smoothness of the mesh-free approximation functions. A formal proof of this is still needed.
3. shape changes can be extreme from one iteration to the next and are no longer limited by differences in node density as was the case for moving-grid EFG-based shape optimization methods.

The method introduced here is applicable to general optimization problems in elasticity, etc. Here, we treated in detail examples from shape optimization of the convective boundary for cooling systems (thermal fins) under natural convection conditions. Sensitivities were computed here, for convenience, internally by the SQP optimizer from the IMSL using finite differences. Compared to previous results on optimal shape design of thermal fins, the newly introduced E(FG)² method proved to be:

– insensitive to the positioning of nodes in the fixed grid,
– capable of handling very large shape changes from one iteration to the next,
– able to enlarge the simple bounds imposed on the shape design variables.

Table 3. Coordinate values of the starting guess (in meters) for the seven design variables (only four a given due to symmetry imposed) used to obtain the optimal shapes in Figures 10 (sharp fins) and 11 (round fins).

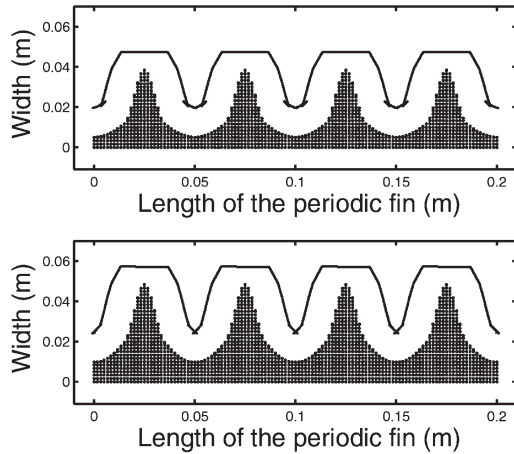| d.v.'s x-coordinates (cm)	d.v.'s y-coordinates for case 1 (cm)	optimal y values for case 1 (cm)	d.v.'s y-coordinates for case 2 (cm)	optimal y values for case 2 (cm)
0.00	0.60	0.50	2.60	0.98
0.50	0.80	0.60	2.80	1.10
1.50	1.50	1.17	3.50	1.96
2.50	3.00	3.85	5.00	4.83

Figure 16. Two local optimal configurations for the periodic fin of a unit conductivity material with an additional constraint for the slope at the ends of the unit cell. Seven design variables are selected on the unit cell (due to symmetry, only four are used). The *top design* (case 1 in Table 3) stays as close as possible to the base of the fin to reduce cooling. The *bottom design* (case 2) produces a similar objective value but uses more area (see Figure 17). The length of the design boundary is longer to compensate for the reduced surface temperature compared to the case 1 design.

We found new characteristics of the solution to the problem of generating optimal shape fins from unfinned areas: low conductivity materials tended to use the maximum amount of cross-sectional area to allow better "access" to the heat source for points on the conductive boundary; whereas, highly conductive materials developed long and narrow fins to maximize the length exposed to the cooling ambient with the design variables touching their lower and upper bounds alternatively, while the cross-sectional area constraint was far from being active. To eliminate boundary overlap in periodic fins, we introduced a new constraint, and we obtained optimal shapes for low conductivity materials in the form of finned cross-sections that are optimal when they remain closer to the heat source.

The shape optimization method developed here was capable of capturing all the essential properties of the problem of shape optimization of cooling systems starting from generic, unfinned shapes. The physical process that determines if fins are to be present or not is driven by the competition between the heat transfer at the convective boundary and the material's conductivity. Several examples from the biological realm can be invoked here in connection to this optimal shape design problem: stegosaurus plates that evolved, at least in part, as heat-loss fins (Farlow et al. 1976), and extended surfaces of intestinal villi. The meaning of the coefficients in the heat transfer equations would have to be changed to describe the mass transfer equations, for the case of the intestinal villi.

Compared to other fictitious-based projection type methods, the E(FG)^2 method introduced here handles large shape changes in fewer iterations and can be applied for shape optimization problems with any types of constraints and boundary conditions.
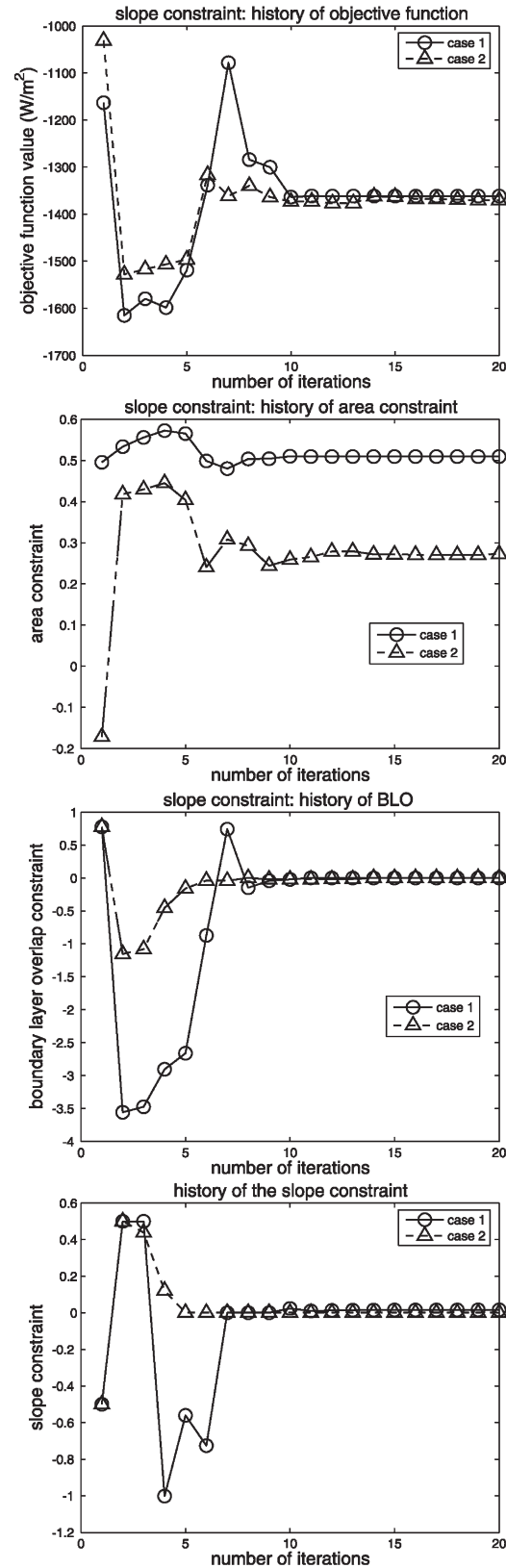

Figure 17. History of the objective function (12) and constraints (13), (14), (15), for a unit-conductivity material with slope constraint. The two starting guesses are as described in Table 3. The design resulting from case 1 is closer to the imposed temperature boundary and uses less area while providing the same heat flux value as that of case 2.

Acknowledgments

References

Belytschko T, Lu YY, Gu L (1994) Element-free Galerkin methods. Int J Numer Methods Eng 37:229–256

Belytschko T, Krongauz Y, Organ D, Fleming M, Krysl P (1996) Meshless methods: An overview and recent developments. Comput Methods Appl Mech Eng 139:3–47

Bobaru F (2001) Meshless methods in shape optimization of linear elastic and thermoelastic solids. Ph.D. dissertation, Cornell University, Ithaca, NY

Bobaru F, Mukherjee S (2001) Shape sensitivity analysis and shape optimization in planar elasticity using the element-free Galerkin method. Comput Methods Appl Mech Eng 190(32–33):4319– 4337

Bobaru F, Mukherjee S (2002) Meshless approach to shape optimization of linear thermoelastic solids. Int J Numer Methods Eng 53(4):765–796

Bobaru F, Rachakonda S (2004a) Boundary layer in shape optimization of convective fins using a meshfree approach. Int J Numer Methods Eng 60(7):1215–1236

Bobaru F, Rachakonda S (2004b) Optimal shape profiles for cooling fins of high and low conductivity. Int J Heat Mass Transfer 47(23):4953–4966

Chen JS, Wang HP (2000) New boundary condition treatments in meshless computation of contact problems. Comput Methods Appl Mech Eng 187:441–468

Duarte CAM (1996) The HP cloud method. Ph.D. dissertation, University of Texas at Austin, Austin, Texas, USA

Farlow JO, Thompson CV, Rosner DE (1976) Plates of stegosaurus. Forced convection heat loss fins? Science 192:1123–1125

Garcia-Ruiz MJ, Steven GP (1999) Fixed grid finite elements in elasticity problems. Eng Comput 16(2–3):145–164

Grindeanu I, Choi KK, Chen JS, Chang KH (1999) Shape design optimization of hyperelastic structures using a meshless method. AIAA J 37(8):990–997

Haslinger J, Mäkinen RAE (2003) Introduction to shape optimization. SIAM, Philadelphia

Haslinger J, Maitre JF, Tomas L (2001a) Fictitious domains methods with distributed Lagrange multipliers Part I: Application to the solution of elliptic state problems. Math Models Methods Appl Sci 11(3):521–547

Haslinger J, Maitre JF, Tomas L (2001b) Fictitious domains methods with distributed Lagrange multipliers Part II: Application to the solution of shape optimization problems. Math Models Methods Appl Sci 11(3):549–563

Kim NH, Choi KK, Botkin ME (2002) Numerical method for shape optimization using meshfree method. Struct Multidisc Optim 24(6):418–429

Mäkinen RAE, Rossi T, Toivanen J (2000) A moving mesh fictitious domain approach for shape optimization problems. Mathematical Modelling and Numerical Analysis 34(1):31–45

Nayroles B, Touzot G, Villon P (1992) Generalizing the finite element method: Diffuse approximation and diffuse elements. Comput Mech 10:307–318

Norato J, Haber R, Tortorelli D, Bendsoe MP (2004) A geometry projection method for shape optimization. Int J Numer Methods Eng 60(14):2289–2312

Rabczuk T, Belytschko T (2005) Adaptivity for structured meshfree particle methods in 2D and 3D. Int J Numer Methods Eng 63(11):1559–1582

Rachakonda S (2003) Optimal shape design of thermal systems with meshfree methods over a fixed grid. Master thesis, University of Nebraska-Lincoln, Lincoln, Nebraska, USA

Turk G, O'Brien JF (2002) Modelling with implicit surfaces that interpolate. ACM Trans Graph 21(4):855–873

White FM (1988) Heat and mass transfer. Addison-Wesley